Copyright © 1997 Elsevier Science Ltd
Int. J. Rock Mech. & Min. Sci. Vol. 34, No. 3-4, 1997 ISSN 0148-9062
To cite this paper: *Int. J. Rock Mech. & Min. Sci.* **34:3–4**, Paper No. 020

Numerical modeling of stress-dependent permeability

M. Bai[1]; F. Meng[1]; D. Elsworth[2]; M. Zaman[3]; J.-C. Roegiers[1]

[1] Rock Mechanics Institute, The University of Oklahoma, Norman, OK 73019, USA

[2] Dept. of Mineral Eng., The Pennsylvania State University, University Park, PA 16802, USA

[3] School of Civil Eng. and Env. Sci., The University of Oklahoma, Norman, OK 73019, USA

ABSTRACT

In this paper, conceptual models are presented to identify the effects of solid deformation on the changes in rock permeabilities for (a) fractured media, (b) intact media, and (c) fractured porous media subjected to external loads, all in steady state conditions. Finite element schemes are then developed with embedded correlations between induced strain and modified permeability to simulate the coupled flow-deformation behavior of reservior rocks tested in the laboratory. Rock specimen permeability is evaluated through comparison between analytical solution and numerical calculation using 'geometric factors'; the latter simulates the actual laboratory experiment where fluid flow and mechanical loading are applied simultaneously on rock samples. Numerical analyses reveal that physical properties of the porous media, including permeability, are significantly altered by mechanical effects, particularly if the media is naturally fractured.

KEYWORDS

Anisotropy • permeability • stress • fluid flow • loading • fractures

1. INTRODUCTION

Permeability controls the rate of fluid transmission in porous and fractured media. Although permeability represents an original geometric property of the porous system, this property can be modified when subjected to variations in stress. Permeability variations may become significant, especially if the porous medium is naturally fractured where the transmissive capacity of highly conductive fractures are extremely sensitive to perturbations in stress.

If permeability is dependent on position within a geological formation, the formation is heterogeneous. Heterogeneities may result from faulting and fracturing induced during subsequent tectonism. Heterogeneities may be present at a variety of length scales, from grain scale of the order of microns to fault zones covering many kilometers. These heterogeneities typically induce a degree of anisotropy that may further control the hydraulic and transport performance of porous and fractured media. The primary cause of anisotropy on a small scale is the orientation of clay minerals in sedimentary rocks and unconsolidated sediments or the alignment of microcracks in indurated materials. Laboratory core samples of clays and shales show horizontal to vertical anisotropy ratios in the range 3:1 to 10:1 (Freeze , Cherry 1979). At a larger scale, field observations indicate a relationship between layered heterogeneity

and anisotropy which may lead to regional anisotropy values on the order of 100:1 or even greater (Maasland 1957; Marcus , Evenson 1961). Snow 1969 showed that fractured rocks behave anisotropically because of the directional variations in fracture aperture and spacing.

Evaluation of anisotropic permeability magnitudes is becoming recognized as increasingly necessary, with core testing techniques providing a viable means to couple this analysis under a varying stress environment (Meng , Bai 1996). In the petroleum industry, interest is motivated from concerns regarding reservoir compaction and the resulting changes in reservoir production that accompany compaction. The present study is motivated from these interests to replicate this field behavior through an investigation of the coupled effect of uniaxial stress on the anisotropic permeabilities of fractured rock specimens in the laboratory.

2. CONCEPTUALIZATION OF STRESS-DEPENDENT PERMEABILITY

Neglecting turbulent flow and assuming flow within a fracture network, Louis 1969 used the parallel plate analog to evaluate the permeability of fracture networks containing a set of regularly spaced parallel fractures subject to steady state fluid flow (Figure 1) as:

$$k = \frac{b^3}{12s} \tag{1}$$

where k is the permeability, b is the fracture aperture, and s is the fracture spacing.

Applying a uniaxial load to the fracture network (Figure 2), Elsworth 1989 derived the permeability change from Eqn. 1, by assuming the individual fractures are distinctly soft with respect to the porous matrix, as:

$$\Delta k = \frac{1}{12s}(b + s\Delta\varepsilon)^3 \tag{2}$$

where $\Delta\varepsilon$ is the elastic strain orthogonal to the fracture network due to application of the load.

For relatively small fracture spacing, Eqn. 2 can be more precisely written as:

$$\Delta k = \frac{1}{12s}[b + (s + b)\Delta\varepsilon]^3 \tag{3}$$

The porous matrix is assumed to be stiff with negligible deformation in the above two equations. If this restriction is released and the contribution of deformations from both fracture and matrix are distinguished and incorporated, the permeability change can be expressed as (Bai , Elsworth 1994):

$$\Delta k = \frac{1}{12s}\left[b + \frac{E(s + b)\Delta\varepsilon}{sK_n + E}\right]^3 \tag{4}$$

where E is the elastic modulus and K_n is the fracture normal stiffness.

For homogeneous nonfractured porous media, the permeability variations can also be associated with the stress change (Figure 3). Instead of change in aperture, changes in either void space or grain volume are

ISSN 0148-9062

the typical consequence that result in permeability changes. Application of Hertz' 1895 elastic contact theory enables permeability change to be expressed as (Bai , Elsworth 1994):

$$\Delta k = k_0 \left\{ 1 \mp \frac{1}{2} \left[\frac{9(1-\nu^2)}{2} (\pi \Delta \varepsilon)^2 \right]^{1/3} \right\}^2 \tag{5}$$

where k_0 is the absolute permeability of the porous medium which can be evaluated using the concept of hydraulic radius (Hubbert 1940; Bear 1972), ν is Poisson ratio. In this equation a negative sign refers to compressional loading while a positive sign corresponds to dilational loading.

In all cases mentioned above, the stress dependent permeability is defined either within the matrix blocks or within the fractures, but not in both spaces. In reality, rock deformation and fluid flow contribute mutually to behavior, as depicted schematically in Figure 4. In combining these effects, three conditions must be simultaneously accommodated: (a) the effective areas of flow are accumulated from both fracture and matrix, i.e., permeability results from the cumulative effect of fracture and matrix permeabilities; (b) elastic strains are individually calculated and superposed through the summation of the respective permeabilities; and (c) load or stress acting on either fracture or matrix is uniform, as required by equilibrium considerations.

To consider the influence of dual-porosity behavior on effective permeability, fracture and porous medium permeabilities are rationed according to their respective initial, in situ, volumes. This rationale is justified since the flow conduits in both porous matrix and fractures are strongly related to the ratio of respective void volume to the total volume (porosity). Using a similar concept as proposed by Kozeny-Carman (Bear 1972), the effective permeability for the dual-porosity medium can be expressed as:

$$\Delta k = \frac{n_1}{n} \Delta k_1 + \frac{n_2}{n} \Delta k_2 \tag{6}$$

where subscripts 1 and 2 represent matrix and fracture, respectively; and the total porosity n is assessed as: $n = n_1 + n_2$. Further in Eqn. 6,

$$\Delta k_1 = k_0 \left\{ 1 \mp \frac{1}{2} \left[\frac{9(1-\nu^2)}{2} (\pi \Delta \varepsilon_1)^2 \right]^{1/3} \right\}^2 \tag{7}$$

where

$$\Delta \varepsilon_1 = \frac{\Delta \sigma}{E} \tag{8}$$

and $\Delta\sigma$ is the total stress change, E and ν must be determined from intact rock containing no fractures.

Also,

$$\Delta k_2 = \frac{1}{12s} [b + (s+b)\Delta \varepsilon_2]^3 \tag{9}$$

ISSN 0148-9062

where

$$\Delta\varepsilon_2 = \frac{\Delta\sigma}{K_n(s+b)} \tag{10}$$

and similarly, K_n must be determined from the fractured rock where deformation of the solid matrix is negligible.

3. NUMERICAL PROCEDURES

For the complex loading geometries and material nonlinearities of 'real' porous media frequently encountered in laboratory experiments, use of numerical schemes such as the finite element method are mandated. In the numerical formulation, the rock deformation and fluid pressure do not interact with each other. The coupling is recovered only through strain-permeability relationship as described previously. The matrix form of the finite element method can be written as:

$$\begin{bmatrix} \mathbf{A} & \mathbf{0} \\ \mathbf{0} & \mathbf{G} \end{bmatrix} \begin{bmatrix} \mathbf{u} \\ \mathbf{p} \end{bmatrix} = \begin{bmatrix} \mathbf{F} \\ \mathbf{Q} \end{bmatrix} \tag{11}$$

where

$$\mathbf{A} = \int_V \mathbf{B}^T \mathbf{D} \mathbf{B} dV \tag{12}$$

$$\mathbf{G} = \frac{1}{\mu} \int_V \nabla \mathbf{M}^T \mathbf{k} \nabla \mathbf{M} dV \tag{13}$$

$$\mathbf{F} = \int_S \mathbf{N} \mathbf{f} dS \tag{14}$$

$$\mathbf{Q} = \int_S \mathbf{M} \mathbf{q} dS \tag{15}$$

where μ is the fluid dynamic viscosity, **N** and **M** are the shape functions for displacements **u** and pressure **p,** within the elements, **B** is the strain-displacement matrix, **A** and **G** are stiffness and conductance matrices, **F** and **Q** are the vectors of applied boundary tractions, **f,** and prescribed nodal fluxes **q,** V and S are the volume and the surface of the domain, and **D** and **k** are the elasticity and the permeability matrices which can be defined as the constants E and k for a one-dimensional case, respectively.

The numerical procedure can be detailed as:

- Derive Δu and Δp from Eqn. 11;
- Calculate strain $\Delta\varepsilon$ from the derived displacement Δu;
- Substitute the strain into the permeability-strain relationships given in the previous section to assess the permeability change Δk;

ISSN 0148-9062

- Determine the change of flow rate using Darcy's law along with derived Δk and Δp, e.g.,

$$\Delta Q = A^* \frac{\Delta k}{\mu} \frac{\Delta p}{L} \tag{16}$$

where L is the flow length, and A^* is the effective flow cross-sectional area. A^* may be determined through examining a 'geometric factor', which relates the numerical solution to the analytical solution (simple uniform stress solution) and is determined by identifying the difference between the flow cross-sectional area A using Darcy's law and the equivalent cross-sectional area A^* in the numerical computation of fluid flow and mechanical loading on a rock specimen. The geometric factor can be defined as $G = A/A^*$. Since the injection area is defined as A, which is relatively small compared to the specimen size, A^* is in general larger than A. As a result, G is usually smaller than 1.

4. DETERMINATION OF STRESS-DEPENDENT PERMEABILITY

As mentioned previously, rock specimen permeability can be determined by performing fluid flow experiments on rock samples in the laboratory. During the test, either flow rate or pressure may be controlled at the fluid injection areas while either pressure or flow rate may be measured at the fluid exit areas. The permeability can then be derived from Darcy's law and through using the concept of the geometric factor described in the last section to compensate for differences between uniform flow in the cross-section evaluated using Darcy's law and the nonuniform flow geometry in the experimental test. Due to rock anisotropy, separate flow tests must be completed to distinguish between vertical and horizontal permeabilities in the specimen. In the following, the behavior of specific rock specimens are evaluated under proposed experimental configurations.

The primary purpose of the present analysis is to determine the effects of stress dependency on permeability variations in three of the four modes depicted in Figures 1–4. In the following, schematic flows through different types of media subjected to uniaxial loading, are labeled as mode-a, mode-b, mode-c, and mode-d, respectively, as shown in Figures 1–1. It should be noted, however, that the proposed models are purely conceptual. They may not represent the actual flow and loading situations, neither the real material structures, nor the present finite element layout. They are designed simply for the interpolation of stress-permeability relationships. The numerical simulations are schematically illustrated in Figure 5, where three-dimensional finite element models in Cartesian coordinate are used. Again, the single-porosity and dual-porosity conceptualizations are represented in the stress-permeability relationship. Basic parameters for the modeling are listed in Table 1. The injection area is confined to represent flow restriction in actual experiments. Flow is maintained at steady state throughout the simulation. Constant rate is applied at the inlet, while the pressure is numerically calculated at the outlet. For simplicity of analysis, the vertical static load is uniaxial on both the top and bottom surfaces of the specimen, which is free to expand laterally as a result of loading.

Comparisons of the pressure -vs- flow-rate (p-q) relationship between the stress-independent permeability (mode-a) and stress-dependent permeability (mode-b) are shown in Figure 6. Several observations may be made as: (a) the pressure -vs- flow-rate relationship is linear, (b) larger permeability magnitudes result in reduced pressure loss, (c) the original fracture permeability (k_0 = 200 md) is assumed to be twice the original matrix permeability (k_0 = 100 md), (d) the matrix is assumed to be impermeable (e.g., no leakoff, or k_z = 0), (e) the loading creates permeability anisotropy that yields k_x =

ISSN 0148-9062

y 0
permeability reduction. The small reduction indicates the reduced influence of loading.

The geometric factor (G-factor) now can be readily derived through comparison between the solutions shown in Figure 6 and the analytical solution (Darcy's law). For k_0 = 100 md, the comparisons of the geometric factors between the mode-b (loading) and the mode-a (no-loading) are given in Figure 7. It is of interest to note that G-factors are independent of the magnitude of flow rates. G-factor for mode-b behavior is always larger than that of mode-a because the effective flow area A^* is always smaller due to the permeability reduction as a result of loading.

In contrast, very little difference is noted in the p-q relationship between the mode-c case, which contains loading, and the case without loading. Because the porous medium is both stiffer and less permeable than the fractured medium, correspondingly, smaller strains and lesser permeability changes are induced. As expected, a neutral result is obtained for the mode-d case, which represents an intermediate medium between the fractured and the intact rocks. Comparisons of the p-q relationship between mode-b, mode-c (no-loading), mode-c (with loading) and mode-d cases are illustrated in Figure 8 for an initial permeability of 100 md for the intact media and 200 md for the fractured media. Different from the impact of loading, there is a significant discrepancy between the fractured and the intact media (e.g., mode-b and mode-c). Comparisons of the geometric factors for different modes are made in Figure 9, which shows consistent patterns in the p-q relationship.

The geometric factors appear to be independent of flow rates. However, these factors may be affected by other influencing variables. Figure 10 illustrates that an increase of a geometric factor is the result of increasing vertical stress and the resulting geometric factor is proportional to the applied uniaxial load. This increase of geometric factor can be attributed to the reduction of the effective cross-sectional area of flow as a result of the incremental enlargement of the mechanical load. It should be noted that the relationship between the geometric factor and the load is nonlinear.

The geometric factors may also be affected by the specimen sizes. For different modes of flow and loading, Figure 11 indicates that the reduction of the geometric factors is associated with the increase of core heights. This increase in core sizes (e.g., heights) leads to an enlarged effective cross-sectional area of flow, and consequently results in a decrease in the geometric factors.

5. CONCLUSIONS

Significant efforts have been made by hydrogeologists, geophysicists, environmentalists, and petroleum engineers to quantify formation permeability, an important parameter in the determination of rate and magnitude of fluid flow through structured porous media. This quantification is further complicated because the original permeability, a geometric quantity, can be significantly modified by other factors of influence, such as mechanical impacts. Several conceptual models, relating rock permeability to mechanical loading in porous and fractured media, are presented in this paper. These conceptualizations are incorporated into finite element models. Numerical schemes are subsequently developed to investigate permeability variations that result when specimens are subjected to changes in external loading during laboratory experiments. The stress-dependent permeability can be determined through comparison between analytical and numerical solutions via a ‘geometric factor’. Numerical simulation of the tests, in which fluid is injected at constant rate into a uniaxially loaded cylindrical rock specimen, reveals a strong correlation between permeability modification and the induced stress. Geometric factors for fractured, intact, and fractured porous media, of various initial permeabilities, subjected to differing

ISSN 0148-9062

external loads are then determined.

ACKNOWLEDGEMENT

Support of the National Science Foundation/State/Industry under the S/IUCRC program and under contract EEC-9209619 is gratefully acknowledged. In particular, the authors want to express their gratitude to Dr. John Dudley from Shell for his valuable input and suggestions. Thanks are also due to the constructive comments and suggestions from Drs. T.E. Scott, Y. Abousleiman and M. Kanj.

FIGURES

Paper 020, Figure 1.

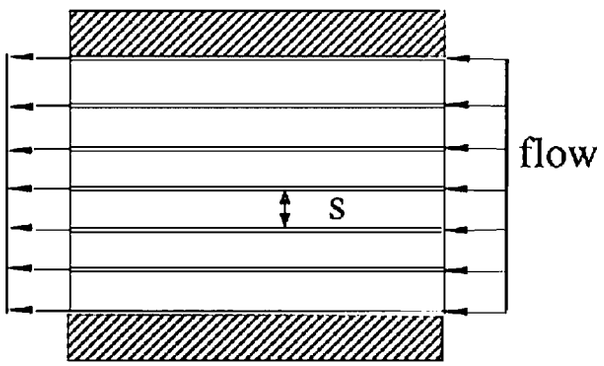

Figure 1. Mode a: flow through fractured media

ISSN 0148-9062

To cite this paper: Int. J. Rock Mech. & Min. Sci. 34:3-4, paper No. 020.

Paper 020, Figure 2.

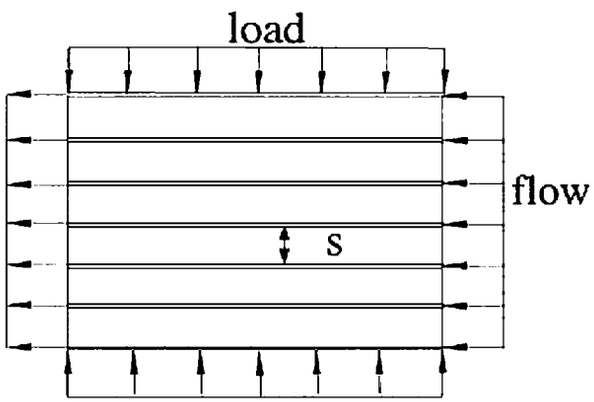

Figure 2. Mode b: flow through loaded fractured media

Paper 020, Figure 3.

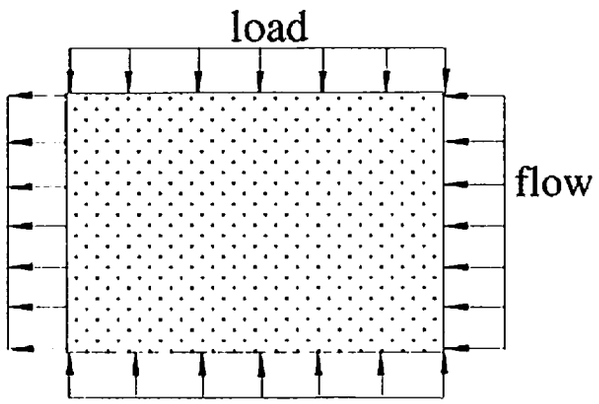

Figure 3. Mode c: flow through loaded porous media

ISSN 0148-9062

To cite this paper: Int. J. Rock Mech. & Min. Sci. 34:3-4, paper No. 020.

Paper 020, Figure 4.

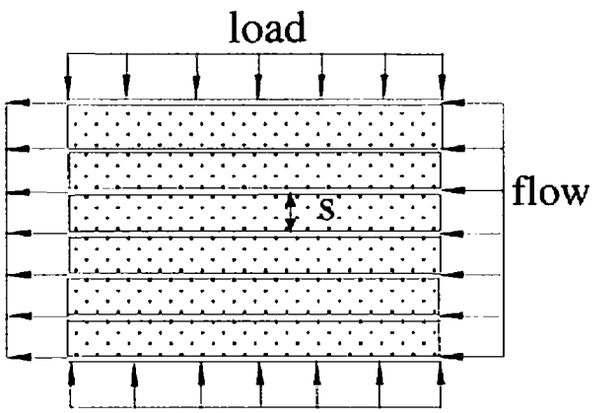

Figure 4. Mode d: flow through loaded fractured porous media

Paper 020, Figure 5.

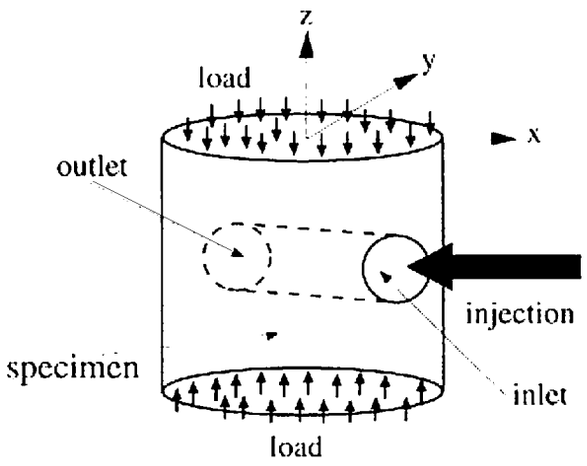

Figure 5. Schematic flow and loading in a rock specimen

ISSN 0148-9062

To cite this paper: Int. J. Rock Mech. & Min. Sci. 34:3-4, paper No. 020.

Paper 020, Figure 6.

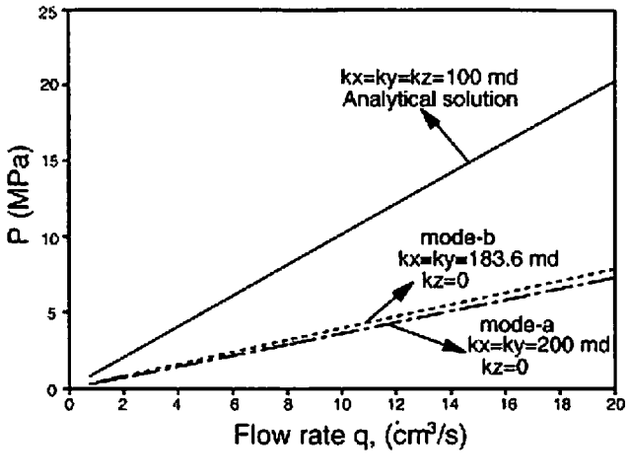

Figure 6. The p-q relationship between mode-a and mode-b cases

Paper 020, Figure 7.

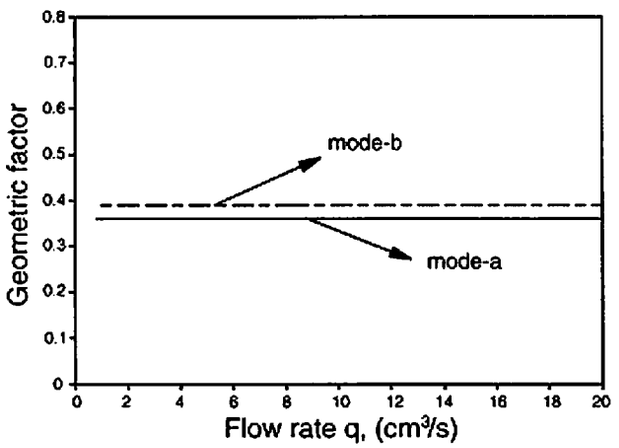

Figure 7. Geometric factors for mode-a and mode-b cases

ISSN 0148-9062

To cite this paper: Int. J. Rock Mech. & Min. Sci. 34:3-4, paper No. 020.

Paper 020, Figure 8.

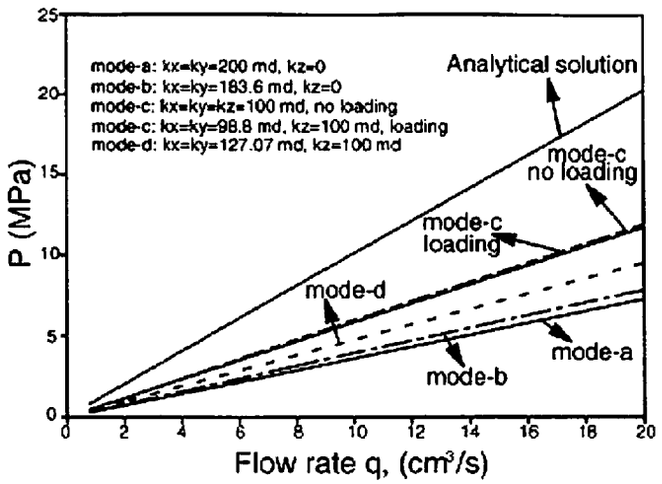

Figure 8. The p-q relationship for various cases

Paper 020, Figure 9.

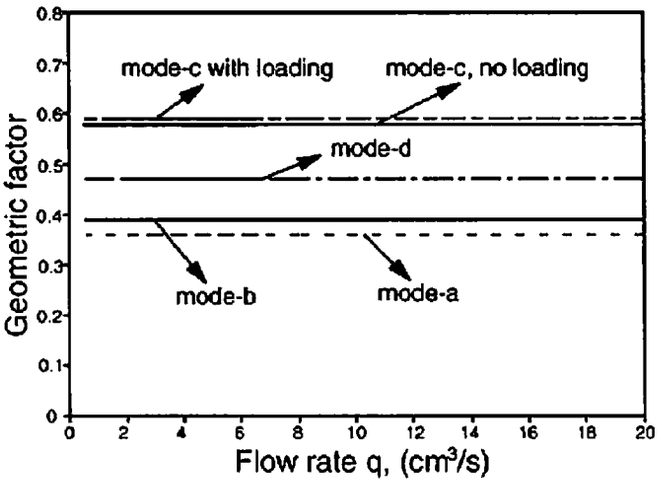

Figure 9. Geometric factors for various cases

ISSN 0148-9062

To cite this paper: Int. J. Rock Mech. & Min. Sci. 34:3-4, paper No. 020.

Paper 020, Figure 10.

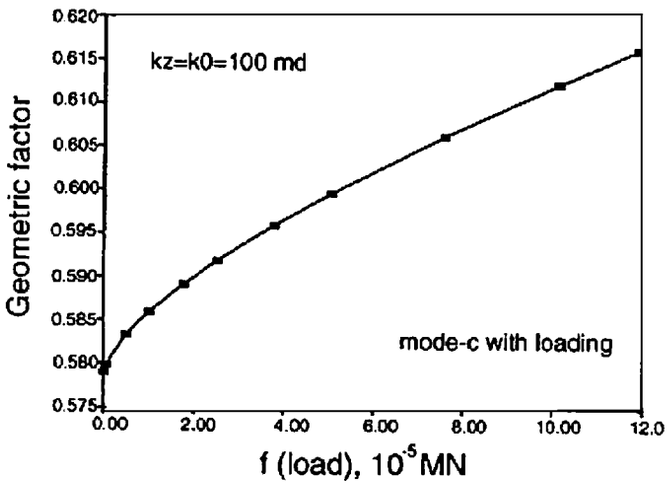

Figure 10. Correlation between geometric factor and loading

Paper 020, Figure 11.

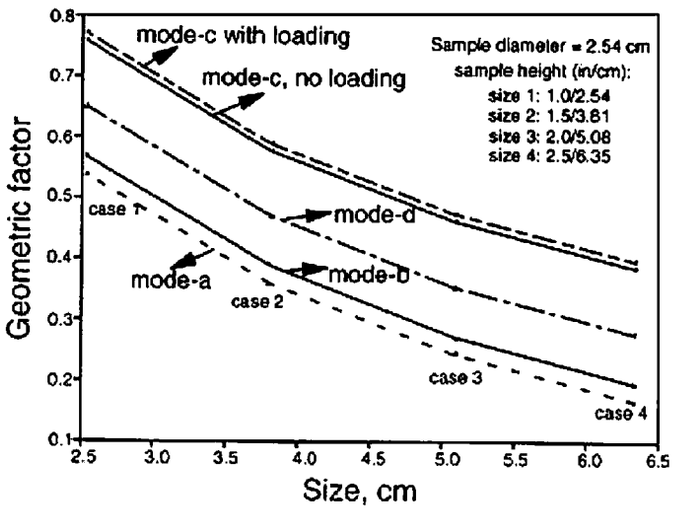

Figure 11. Correlation between geometric factor and specimen geometry

ISSN 0148-9062

To cite this paper: Int. J. Rock Mech. & Min. Sci. 34:3-4, paper No. 020.

TABLES

Paper 020, TABLE 1.

TABLE 1
SELECTED PARAMETERS FOR MODELING

Parameter	Unit	Mode-a	Mode-b	Mode-c (no-F)	Mode-c (F)	Mode-d
Flow rate Q	cm^3/s	0.8-2	0.8-2	0.8-2	0.8-2	0.8-2
External load F	MN	-	1e-5	-	1e-5	1e-5
Elastic modulus E	MN/m^2	100	100	100	100	100
Poisson's ratio ν	-	0.25	0.25	0.25	0.25	0.25
Fracture stiffness K_n	$MN/m^2/m$	100	100	-	-	100
Matrix porosity n_1	-	-	-	0.1	0.1	0.1
Fracture porosity n_2	-	0.05	0.05	-	-	0.05
Matrix permeability k_1	md	-	-	100	100	100
Fracture permeability k_2	md	200	200	-	-	200
Fluid viscosity μ	cp	0.5	0.5	0.5	0.5	0.5
Fracture spacing s	cm	0.254	0.254	-	-	0.254

References

References

Bai M., Elsworth D. 1994. Modeling of subsidence and stress-dependent hydraulic conductivity of intact and fractured porous media, *Rock Mech. and Rock Engng.*, **27:4,** 209–234.

Bear J. 1972. *Dynamics of Fluids in Porous Media,* American Elsevier Publishing Company, Inc., NY, 764p.

Elsworth D. 1989. Thermal permeability enhancement of blocky rocks: one-dimensional flows, *Int. J. Rock Mech. Min. Sci. and Geomech. Abstr.,* **26:3/4,** 329–339.

Freeze R. A., Cherry J. A. 1979. *Groundwater,* Prentice-Hall, Inc., Englewood Cliffs, New Jersey, USA.

Hertz 1895. *Collected Works,* 179–195, in German.

Hubbert M. K. 1940. The theory of groundwater motion, *J. Geol.,* **48:** 785–822.

Louis C. 1969. Groundwater flow in rock masses and its influence on stability, *Rock Mech. Research Report,* no.10, Imperial College, UK.

Maasland M. 1957. Soil anisotropy and land drainage, *Drainage of Agricultural Lands,* ed. J. N. Luthin, ASA, Madison, Wis., 216–285.

Marcus H., Evenson D. E. 1961. Directional permeability in anisotropic porous media, *Water Resources Center Contrib.,* No. 31, University of California, Berkeley.

ISSN 0148-9062

To cite this paper: Int. J. Rock Mech. & Min. Sci. 34:3-4, paper No. 020.

Meng F., Bai M. 1996. Study of radial fluid flow in anisotropic media: numerical approach, Report RMC-96–06.

Snow D. T. 1969. Anisotropic Permeability of Fractured Media, *Water Resources Research,* **5:6,** 1273–1289.

ISSN 0148-9062